#### Accepted Manuscript

Protein-Solvent Interfaces in Human Y145Stop Prion Protein Amyloid Fibrils Probed by Paramagnetic Solid-State NMR Spectroscopy

Darryl Aucoin, Yongjie Xia, Theint Theint, Philippe S. Nadaud, Krystyna Surewicz, Witold K. Surewicz, Christopher P. Jaroniec

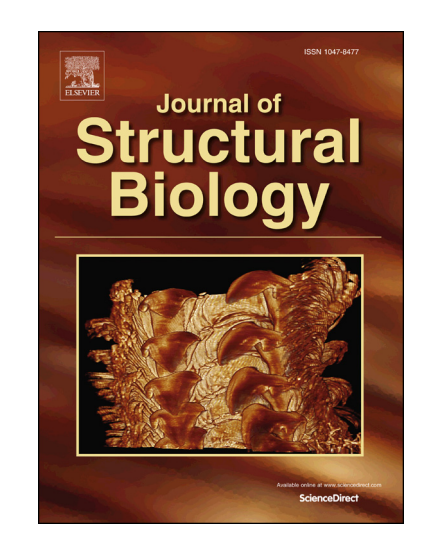
PII: S1047-8477(18)30092-3

DOI: https://doi.org/10.1016/j.jsb.2018.04.002

Reference: YJSBI 7182

To appear in: Journal of Structural Biology

Received Date: 25 February 2018 Revised Date: 24 March 2018 Accepted Date: 13 April 2018



Please cite this article as: Aucoin, D., Xia, Y., Theint, T., Nadaud, P.S., Surewicz, K., Surewicz, W.K., Jaroniec, C.P., Protein-Solvent Interfaces in Human Y145Stop Prion Protein Amyloid Fibrils Probed by Paramagnetic Solid-State NMR Spectroscopy, *Journal of Structural Biology* (2018), doi: https://doi.org/10.1016/j.jsb.2018.04.002

This is a PDF file of an unedited manuscript that has been accepted for publication. As a service to our customers we are providing this early version of the manuscript. The manuscript will undergo copyediting, typesetting, and review of the resulting proof before it is published in its final form. Please note that during the production process errors may be discovered which could affect the content, and all legal disclaimers that apply to the journal pertain.

# Protein-Solvent Interfaces in Human Y145Stop Prion Protein Amyloid Fibrils Probed by Paramagnetic Solid-State NMR Spectroscopy

Darryl Aucoin,<sup>a</sup> Yongjie Xia,<sup>a</sup> Theint Theint,<sup>a</sup> Philippe S. Nadaud,<sup>a</sup> Krystyna Surewicz,<sup>b</sup> Witold K. Surewicz,<sup>b</sup> and Christopher P. Jaroniec<sup>a,\*</sup>

<sup>a</sup>Department of Chemistry and Biochemistry, The Ohio State University,
Columbus, OH 43210, USA
<sup>b</sup>Department of Physiology and Biophysics, Case Western Reserve University,
Cleveland, OH 44106, USA

Corresponding author email: jaroniec.1@osu.edu

#### Abstract

The C-terminally truncated Y145Stop variant of prion protein (PrP23-144), which is associated with heritable PrP cerebral amyloid angiopathy in humans and also capable of triggering a transmissible prion disease in mice, serves as a useful in vitro model for investigating the molecular and structural basis of amyloid strains and cross-seeding specificities. Here, we determine the protein-solvent interfaces in human PrP23-144 amyloid fibrils generated from recombinant <sup>13</sup>C, <sup>15</sup>N-enriched protein and incubated in aqueous solution containing paramagnetic Cu(II)-EDTA, by measuring residue-specific <sup>15</sup>N longitudinal paramagnetic relaxation enhancements using two-dimensional magic-angle spinning solid-state NMR spectroscopy. To further probe the interactions of the amyloid core residues with solvent molecules we perform complementary measurements of amide hydrogen/deuterium exchange detected by solid-state NMR and solution NMR methods. The solvent accessibility data are evaluated in the context of the structural model for human PrP23-144 amyloid.

**Keywords:** Prions; Amyloids; Protein aggregation; Paramagnetic solid-state NMR; Hydrogen/deuterium exchange

#### Introduction

The prion diseases, which include Creutzfeld-Jakob disease and bovine spongiform encephalopathy, are a family of lethal neurodegenerative disorders that have been linked to the conformational conversion of prion protein (PrP), a largely  $\alpha$ -helical brain glycoprotein, from its native monomeric form (PrP<sup>C</sup>) to supramolecular  $\beta$ -sheet-rich aggregates (PrP<sup>Sc</sup>) (Aguzzi et al., 2008; Cobb and Surewicz, 2009; Kraus et al., 2013; Prusiner, 1998). Although currently not fully understood at the molecular level, prion infectivity and ability to be transmitted between different hosts appears to be closely tied to the three-dimensional structures of fibrillar PrP<sup>Sc</sup> deposits (Aguzzi et al., 2008; Bett et al., 2012; Caughey et al., 1998; Cobb and Surewicz, 2009; Collinge and Clarke, 2007; Peretz et al., 2002; Safar et al., 1998; Surewicz and Apostol, 2011).

We have previously shown that the Y145Stop mutant of prion protein (PrP23-144), which is associated with a familial human prionopathy (Ghetti et al., 1996; Kitamoto et al., 1993), is a valuable model for investigating the molecular basis of amyloid and prion propagation phenomena including strains and species barriers (Jones and Surewicz, 2005; Kundu et al., 2003; Surewicz et al., 2006; Vanik et al., 2004). Recent studies also indicate that synthetic mouse PrP23-144 amyloids are infectious and capable of causing transmissible prion disease in mice (Choi et al., 2016). In order to gain an in-depth understanding of the molecular and structural basis of Y145Stop PrP amyloid propagation we have undertaken high-resolution solid-state nuclear magnetic resonance (NMR) studies of recombinant amyloid fibrils formed by a set of related mammalian (human, mouse and Syrian hamster) PrP23-144 proteins exhibiting a high degree of sequence identity (Helmus et al., 2010; Helmus et al., 2008; Helmus et al., 2011; Jones et al., 2011; Theint et al., 2017a; Theint et al., 2017b). These studies permitted an initial structural model to be proposed for human PrP23-144 (huPrP23-144) amyloid, where the fibrils

contain two protofilaments in a C<sub>2</sub>-symmetric arrangement with each protofilament consisting of a relatively rigid parallel-in-register β-core of ~30 amino acid residues located near the C-terminus and a disordered flexible N-terminal tail region (Theint et al., 2017b). Furthermore, we found that human and mouse PrP23-144 are able to adopt similar, albeit distinct, conformations in the amyloid state that differ considerably from the conformation of the Syrian hamster fibrils, and showed that these conformational preferences, as well as the ability of the mouse and Syrian hamster PrP23-144 to misfold into multiple amyloid strains with different structures, are primarily governed by the identities of two amino acids at positions 112 and 139 (Theint et al., 2017a; Theint et al., 2017b). Here, as part of our ongoing efforts to elucidate the three-dimensional structures of mammalian Y145Stop PrP amyloids, we report our characterization of the fibril-solvent interfaces in huPrP23-144 amyloid by using paramagnetic solid-state NMR methods in combination with NMR-detected hydrogen/deuterium (H/D) exchange and interpret these solvent-accessibility data in the context of the current structural model of the huPrP23-144 fibril core.

#### **Materials and Methods**

*Preparation of human PrP23-144 amyloid fibrils.* Recombinant <sup>13</sup>C, <sup>15</sup>N-enriched human PrP23-144 was expressed in *E. coli* BL21(DE3) strain and purified as described previously (Theint et al., 2017a; Theint et al., 2017b). Amyloid fibrils were generated at 25 °C under quiescent conditions (Theint et al., 2017a; Theint et al., 2017b) by dissolving purified lyophilized huPrP23-144 in ultrapure water at a concentration of 400 μM (~5 mg/mL), and adding 1 M potassium phosphate pH 6.4 buffer to a final concentration of 50 mM as well as 1% (v/v) of an aqueous solution containing preformed huPrP23-144 amyloid fibril seeds at a concentration of

 $400~\mu M$  in 50 mM potassium phosphate pH 6.4 buffer. Following an incubation period of 24 h the fibrils were washed with two aliquots of 50 mM potassium phosphate pH 6.4 buffer, pelleted using a tabletop centrifuge, and either transferred to 3.2 mm Bruker solid-state NMR zirconia rotors (reference sample) or treated further as described below. Each of the samples used for the solid-state NMR measurements contained ~10 mg of fibrils.

Cu(II)-EDTA doped amyloid fibrils for solid-state NMR. The huPrP23-144 fibrils were incubated for 48 h at 4 °C in 50 mM potassium phosphate pH 6.4 buffer containing Cu(II)-EDTA at a concentration of 20 mM or 200 mM, washed with two aliquots of 50 mM potassium phosphate pH 6.4 buffer containing Cu(II)-EDTA at the desired concentration (20 or 200 mM), and transferred by centrifugation to 3.2 mm Bruker solid-state NMR zirconia rotors.

Amyloid fibrils for hydrogen/deuterium exchange solid-state NMR. The pelleted huPrP23-144 fibrils were rapidly washed at 4 °C with two aliquots of 50 mM potassium phosphate buffer in D<sub>2</sub>O (pD\* 6.5) to remove residual bulk H<sub>2</sub>O, and subsequently incubated at 25 °C for 2, 6 or 48 h in excess D<sub>2</sub>O-based 50 mM potassium phosphate buffer. The fibrils were then transferred by centrifugation to 3.2 mm Bruker solid-state NMR zirconia rotors.

Samples for hydrogen/deuterium exchange solution NMR. The pelleted huPrP23-144 fibrils were rapidly washed at 4 °C with two aliquots of 50 mM potassium phosphate buffer in D<sub>2</sub>O (pD\* 6.5) to remove residual bulk H<sub>2</sub>O, and subsequently incubated at 25 °C for 1, 6, 24, 72 or 168 h in excess D<sub>2</sub>O-based 50 mM potassium phosphate buffer. Following the incubation period the fibrils were pelleted using a tabletop centrifuge and lyophilized. The lyophilized fibrils were then dissolved to a final concentration of 0.6 mM in a buffer solution containing 95% (v/v) d<sub>6</sub>-DMSO, 4.5% (v/v) D<sub>2</sub>O and 0.5% (v/v) d<sub>2</sub>-dichloroacetic acid at pD\* 5.0 and loaded into Shigemi microcells (~300 μL volume) for immediate analysis by solution NMR.

Avance III HD spectrometer equipped with a 3.2 mm Efree HCN probe. The magic angle spinning frequency was set to 11.111 kHz and the effective sample temperature was maintained at ~5 °C. 2D <sup>15</sup>N-<sup>13</sup>Cα chemical shift correlation spectra, with short (180 μs) <sup>1</sup>H-<sup>15</sup>N cross polarization contact times to minimize polarization transfer to amide <sup>15</sup>N nuclei from aliphatic protons or amide protons of adjacent residues, were recorded for samples incubated in the D<sub>2</sub>O-based potassium phosphate buffer for increasing amounts of time to assess the extent of H/D exchange in the fibril core. The residue-specific longitudinal <sup>15</sup>N relaxation rate constants as a result of exposure to Cu(II)-EDTA in the solvent were determined as described previously (Nadaud et al., 2009; Sengupta et al., 2012), based on a series of 2D <sup>15</sup>N-<sup>13</sup>Cα correlation spectra recorded with longitudinal relaxation delays of 10 μs, 0.5 s, 1 s, 2 s and 4 s. All solid-state NMR data were processed in NMRPipe (Delaglio et al., 1995) and the longitudinal relaxation data were analyzed using nmrglue (Helmus and Jaroniec, 2013).

Solution NMR spectroscopy. NMR measurements were performed at 25 °C on an 800 MHz Bruker Avance III HD spectrometer equipped with a cryogenic probe with z-axis gradients. Spectra were processed using NMRPipe (Delaglio et al., 1995) and analyzed using Sparky (Goddard and Kneller, 2006) and nmrglue (Helmus and Jaroniec, 2013).

Sequential backbone resonance assignments of huPrP23-144 in a DMSO-based buffer solution, analogous to the one used to dissolve amyloid fibril samples for the H/D exchange measurements described below, were established using <sup>13</sup>C, <sup>15</sup>N-labeled protein and 3D HNCO, HNCA and HN(CA)CB pulse sequences based on the schemes of Kay and co-workers (Yamazaki et al., 1994).

In order to assess the extent of residue-specific amide H/D exchange, corrected for any possible amide proton exchange with the  $d_6$ -DMSO,  $D_2O$ ,  $d_2$ -dichloroacetic acid dissolution buffer (Luhrs et al., 2005), a series of 20  $^{15}N^{-1}H$  heteronuclear single quantum coherence (HSQC) spectra with duration of ~15 minutes each were recorded for huPrP23-144 fibril samples incubated in the  $D_2O$ -based potassium phosphate buffer for varying amounts of time as described above. Following these measurements, a 1D  $^{1}H$  spectrum was recorded for each sample, with the total spectral intensity in the region corresponding to non-exchangeable aliphatic protons used to assess the protein concentration and normalize the residue-specific H/D exchange data for the different samples.

#### **Results and Discussion**

Fibril-solvent interfaces probed by paramagnetic solid-state NMR. Previous studies indicate that huPrP23-144 amyloid fibrils are composed of two protofilaments (Theint et al., 2017b), with residues ~112-141 of each protofilament forming a relatively rigid parallel-in-register β-core and the remaining residues being dynamically disordered (Helmus et al., 2010; Helmus et al., 2008; Helmus et al., 2011). In order to directly probe the protein-solvent interfaces in huPrP23-144 amyloid, we monitored the <sup>15</sup>N longitudinal relaxation rates of individual residues in the β-core for fibril samples incubated with 20 or 200 mM Cu(II)-EDTA. Similar approaches have been previously successfully used in studies of other peptide and protein assemblies including amyloid fibrils (Linser et al., 2009; Oster et al., 2017; Wickramasinghe et al., 2009). Figure 1 shows representative fingerprint 2D <sup>15</sup>N-<sup>13</sup>Cα chemical shift correlation spectra, with <sup>15</sup>N longitudinal relaxation delays of 10 μs (Figure 1A) and 2 s (Figure 1B) prior to <sup>15</sup>N chemical shift encoding (Nadaud et al., 2009), recorded for huPrP23-144 amyloid fibrils

incubated in phosphate buffer solution containing 200 mM Cu(II)-EDTA; additional <sup>15</sup>N-<sup>13</sup>Cα spectra for fibrils incubated with 20 mM Cu(II)-EDTA are shown in Supporting Information (SI) Figure S1. These spectra indicate that, relative to the control huPrP23-144 amyloid sample containing no Cu(II)-EDTA, for fibrils incubated with 20 or 200 mM Cu(II)-EDTA roughly half of the resonances experience significant longitudinal amide <sup>15</sup>N paramagnetic relaxation enhancements (PREs), as manifested by major suppression of cross-peak intensities in the spectra recorded with the longer relaxation delays, caused by the close proximity of these protein <sup>15</sup>N nuclei to the paramagnetic Cu<sup>2+</sup> centers present in the solvent.

Figure 1C shows the amide <sup>15</sup>N longitudinal relaxation trajectories for representative residues in huPrP23-144 fibrils incubated with 20 and 200 mM Cu(II)-EDTA; the complete set of relaxation trajectories is shown in SI Figure S2. In Figure 3A we show a plot of the longitudinal <sup>15</sup>N PREs as a function of residue number, calculated by subtracting the longitudinal <sup>15</sup>N relaxation rate constants (R<sub>1</sub>) for the paramagnetic and diamagnetic samples. These data indicate that the smallest <sup>15</sup>N PREs (less than ~0.1-0.2 s<sup>-1</sup>) are observed for residues 115-127, while, on the whole, residues 113-114 and 130-141 experience the most pronounced relaxation enhancements in the ~0.3-0.6 s<sup>-1</sup> regime. Furthermore, for the majority of residues, the bulk of the observed relaxation enhancements are realized already in the presence of 20 mM Cu(II)-EDTA, with relatively minor additional PRE effects when the Cu<sup>2+</sup> concentration is increased ten-fold to 200 mM. Altogether, these results clearly indicate that the amyloid core residues 113, 114 and 130-141 are the most solvent-exposed and presumably located at or near the fibril-solvent interfaces, while residues 115-127 are located in part of the core that is relatively protected from the solvent.

Fibril-solvent interfaces probed by hydrogen/deuterium exchange. Hydrogen/deuterium exchange of backbone amide groups can provide an additional measure of solvent accessibility, even though interpretation of exchange data is more complicated as the exchange rates are affected both by solvent accessibility as well as the presence (and stability) of hydrogen bonds within secondary structure elements such as α-helices and β-sheets (Englander and Kallenbach, 1983). To corroborate the results of the paramagnetic solid-state NMR experiments we investigated the extent of amide H/D exchange for individual residues in huPrP23-144 amyloid, by incubating the fibrils in D<sub>2</sub>O-based potassium phosphate buffer at 25 °C for varying amounts of time and monitoring the changes in signal intensities on a residue-specific basis using 2D solid-state NMR (Chevelkov et al., 2017; Cotten et al., 1999; del Amo et al., 2010; Grohe et al., 2017; Sharpe et al., 2006; Wang et al., 2011).

In Figure 2 we compare the fingerprint 2D  $^{15}$ N- $^{13}$ C $\alpha$  solid-state NMR spectrum recorded for huPrP23-144 fibrils subjected to H/D exchange in the D<sub>2</sub>O-based buffer for 48 h with a reference 2D  $^{15}$ N- $^{13}$ C $\alpha$  spectrum for fibrils not exposed to D<sub>2</sub>O. Additional 2D  $^{15}$ N- $^{13}$ C $\alpha$  spectra for huPrP23-144 fibril samples that have undergone H/D exchange for 2 h and 6 h are shown in SI Figure S3. Note that these data were recorded at a temperature of ~5 °C, where the amide hydrogen exchange rate is significantly reduced relative to ambient conditions (Englander et al., 1972). Moreover, the data were collected as a series of 2D  $^{15}$ N- $^{13}$ C $\alpha$  spectra with relatively short experiment times (~3 h), which enabled us to confirm directly that no appreciable H/D exchange occurred during the course of the solid-state NMR experiments. In these 2D  $^{15}$ N- $^{13}$ C $\alpha$  spectra, for each amino acid residue, the nuclear spin magnetization is initially transferred from the amide  $^{1}$ H to  $^{15}$ N and subsequently to the directly bonded  $^{13}$ C $\alpha$  for detection. The use of a  $^{1}$ H- $^{15}$ N cross-polarization period of minimal duration needed for efficient magnetization transfer (180

 $\mu$ s) ensures that the vast majority of the proton magnetization that is transferred to each amide  $^{15}$ N, and ultimately  $^{13}$ C $\alpha$ , originates from the amide  $^{1}$ H for that residue as opposed to aliphatic protons or amide protons of neighboring residues. Consequently, the intensities of  $^{15}$ N- $^{13}$ C $\alpha$  correlations for residues where a certain fraction of the amide protons has been exchanged for  $^{2}$ H (on average for the macroscopic sample) are expected to be proportionally reduced.

As summarized in Figure 3B, these data indicate that one contiguous stretch of the protein sequence spanning residues 115-125 displays the highest overall cross-peak intensities for fibril samples that have been incubated in D<sub>2</sub>O relative to the control sample. After 2 h and 48 h of H/D exchange residues located within this segment respectively retain ~80% and ~50% of their intensity on average relative to the control sample, and thus appear to be the most strongly protected from exchange. In contrast, many residues located outside this region (113-114, 132-135, 141) have lower signal intensities upon exposure to D<sub>2</sub>O, with several residues (G114, S132 and F141) being particularly susceptible to H/D exchange and showing severely reduced intensities even for the shortest, 2 h, incubation time. Note that G114 and F141 are located near the N- and C-terminal edges of the huPrP23-144 amyloid fibril core, respectively (Theint et al., 2017b), while the exchange rate for the S132 amide proton may be further accelerated due to the polar nature of its side-chain (Bai et al., 1993) that is likely to be solvent exposed (Theint et al., 2017b). Overall, these results are in reasonable agreement with the analysis of protein-solvent interfaces based on measurements of amide <sup>15</sup>N longitudinal PREs in huPrP23-144 amyloid samples incubated with Cu(II)-EDTA (vide supra), which suggests that residues 115-127 constitute the most solvent-protected part of the fibril core.

Finally, in addition to directly probing the extent of H/D exchange for huPrP23-144 amyloid core residues using solid-state NMR and intact fibril samples as described above, we

performed a set of complementary experiments where H/D exchange is monitored in a residue-specific manner by <sup>15</sup>N-<sup>1</sup>H HSQC solution NMR following the dissolution in a DMSO-based buffer of fibril samples exposed to D<sub>2</sub>O for varying amounts of time. This type of approach has been previously employed to investigate amyloid fibrils formed by multiple peptides and proteins (Hoshino et al., 2007), including PrP fragments 106-126 (Kuwata et al., 2003), 89-143 (P101L mutant) (Damo et al., 2010) and 23-159 (Skora et al., 2013). H/D exchange times ranging from 1 to 168 h were investigated, and for most residues the exchange process was found to be effectively complete within ~24-48 h.

SI Figure S4 shows <sup>15</sup>N-<sup>1</sup>H HSQC spectra of huPrP23-144 fibrils dissolved in the pD\* 5.0 d<sub>6</sub>-DMSO based buffer containing 4.5% D<sub>2</sub>O, corresponding to no H/D exchange in D<sub>2</sub>Obased potassium phosphate buffer (reference sample) and H/D exchange times of 1 h and 6 h. Given that the experiment "dead-time" required for dissolution of the fibrils and NMR experiment set up was ~15 minutes and that non-negligible further amide H/D exchange generally occurs in the DMSO-based quenching buffer (Hoshino et al., 2007; Luhrs et al., 2005), the residue-specific proton occupancies at time zero of the measurement were extrapolated from spectral intensities in series of successive HSQC spectra recorded as described in the Materials and Methods section (see SI Figure S5 for representative data). In SI Figure S6 we show the H/D exchange trajectories for the huPrP23-144 amyloid core residues, as well as several representative residues located outside the core region. For all residues located outside the core the H/D exchange was very rapid and typically complete within 6 h. Similar rapid exchange profiles were also observed for residues found at the edges of the core (A113, G114, F141 and G142), as well as for several residues within the core including S132 and S135. For most of the remaining amyloid core residues (A115-H140) the exchange profiles displayed reduced initial

exchange rates and/or significantly higher steady-state proton occupancies, and appeared to contain contributions from two components with different exchange rates. Note that such two-component H/D exchange profiles, consisting of a rapidly exchanging component and a very slowly exchanging component, have been reported for a number of other amyloids investigated by using this methodology (for example (Hoshino et al., 2007; Luhrs et al., 2005)) and generally attributed to several possible factors including exchange between the fibril and soluble states of protein molecules located at the fibril edges, fibril structural heterogeneity and/or presence of residual protein oligomers in the fibril sample. A summary of these data is presented in Figure 3C, which shows the relative amide cross-peak intensities for the huPrP23-144 amyloid core residues as a function of residue number for H/D exchange times of 1, 6 and 24 h. While these data are generally consistent with the results of the solvent PRE and H/D exchange solid-state NMR experiments in terms of identifying the huPrP23-144 residues making up the amyloid core region, in and of themselves they do not appear to enable the most solvent exposed and protected residues within the core to be readily classified in an unambiguous manner.

Summary of solvent accessibility data and relation to structural model. Figure 3A-C shows a summary of all the solvent accessibility data for the amyloid core residues in huPrP23-144 fibrils. Taken together, these data indicate that residues 115-127 are relatively solvent-protected, amino acids 113-114 and 141 are the most solvent-exposed, and residues within the 130-140 region show variable degree of solvent accessibility. Importantly, these results are consistent with and provide further independent validation for the structural model of huPrP23-144 amyloid fibrils shown in Figure 3D, according to which the fibrils consist of two protofilaments in a  $C_2$ -symmetric arrangement with parallel in-register  $\beta$ -sheet regions running parallel to the long fibril axis (Theint et al., 2017b). Specifically, in this structural model the

hydrophobic alanine, glycine, leucine and valine residues (amino acids  $\sim$ 115-127) are located at the interface between the two protofilaments in the interior of the fibril core, where they are relatively shielded from direct contacts with solvent. On the other hand, residues  $\sim$ 130-140 make up the extended C-terminal  $\beta$ -strands positioned at the exterior of the fibril, where they are more readily accessible to solvent molecules. This may explain why, despite the network of stabilizing hydrogen bonds, some residues in this region show little protection from H/D exchange. Not surprisingly, little protection from exchange (and high solvent accessibility as probed by paramagnetic solid-state NMR) is also observed for residues 113-114 and 141 that are located near the amyloid core boundaries.

Our findings are also generally consistent with the studies of human PrP23-159 amyloid by Skora et al. (Skora et al., 2013) using H/D exchange coupled with solution NMR spectroscopy and hydroxyl radical footprinting detected by mass spectrometry, which localized the fibril core region to residues 109-142 and pointed to the side-chain of residue 129 as being buried within this core. Although our solid-state NMR experiments are not able to directly probe the solvent PRE and H/D exchange for the amide of residue M129, which is undetectable in conventional solid-state NMR spectra of huPrP23-144 fibrils due to the flexibility of the protein backbone at that site (Helmus et al., 2010; Helmus et al., 2008; Helmus et al., 2011), the structural model of huPrP23-144 amyloid in Figure 3D indicates that it is feasible for the M129 side-chain to be readily accommodated within the interior of the fibril core. Additionally, previous studies of mouse PrP106-126 fibrils by H/D exchange coupled to solution NMR (Kuwata et al., 2003) concluded that residues 111-123 comprise the most solvent protected part of the amyloid β-core region. While this result is also consistent with our findings for human PrP23-144 fibrils, this correspondence may be coincidental in nature given that the structural

models proposed for the mouse PrP106-126 fibrils (Kuwata et al., 2003) and homologous human PrP106-126 fibrils (Walsh et al., 2009) differ significantly from the conformation adopted by these residues in huPrP23-144 fibrils and their location within the amyloid core according to our structural model. Interestingly, our findings differ somewhat from the results of H/D exchange measurements for fibrils formed by the P101L mutant of mouse PrP89-143 (Damo et al., 2010), where residues 102-109 and 117-136 were found to display high levels of protection from exchange with solvent. A possible reason for this discrepancy is that this particular PrP fragment forms a structure in the amyloid state that differs considerably from those of human or mouse PrP23-144 investigated in our studies, both of which adopt similar fibril conformations (Theint et al., 2017a; Theint et al., 2017b). Indeed, earlier solid-state NMR studies of mouse PrP89-143 fibrils (Laws et al., 2001; Lim et al., 2006) suggest that this may be the case.

#### Acknowledgements

This research was supported by the National Science Foundation (grants MCB-1243461 and MCB-1715174 to C.P.J.), the National Institutes of Health (grants R01GM094357 and S10OD012303 to C.P.J. and P01AI106705 and R01NS083687 to W.K.S.) and the Camille & Henry Dreyfus Foundation (Camille Dreyfus Teacher-Scholar Award to C.P.J).

#### **Supporting Information**

Supporting information accompanies this paper at doi: ...

#### References

- Aguzzi, A., Sigurdson, C., Heikenwaelder, M., 2008. Molecular mechanisms of prion pathogenesis. Annu. Rev. Pathol. 3, 11-40.
- Bai, Y., Milne, J.S., Mayne, L., Englander, S.W., 1993. Primary structure effects on peptide group hydrogen exchange. Proteins 17, 75-86.
- Bett, C., Joshi-Barr, S., Lucero, M., Trejo, M., Liberski, P., Kelly, J.W., Masliah, E., Sigurdson, C.J., 2012. Biochemical properties of highly neuroinvasive prion strains. PLoS Pathog. 8, e1002522.
- Caughey, B., Raymond, G.J., Bessen, R.A., 1998. Strain-dependent differences in β-sheet conformations of abnormal prion protein. J. Biol. Chem. 273, 32230-32235.
- Chevelkov, V., Giller, K., Becker, S., Lange, A., 2017. Measurement of backbone hydrogendeuterium exchange in the type III secretion system needle protein PrgI by solid-state NMR. J. Magn. Reson. 283, 110-116.
- Choi, J.K., Cali, I., Surewicz, K., Kong, Q., Gambetti, P., Surewicz, W.K., 2016. Amyloid fibrils from the N-terminal prion protein fragment are infectious. Proc. Natl. Acad. Sci. USA 113, 13851-13856.
- Cobb, N.J., Surewicz, W.K., 2009. Prion diseases and their biochemical mechanisms. Biochemistry-Us 48, 2574-2585.
- Collinge, J., Clarke, A.R., 2007. A general model of prion strains and their pathogenicity. Science 318, 930-936.
- Cotten, M., Fu, R., Cross, T.A., 1999. Solid-state NMR and hydrogen-deuterium exchange in a bilayer-solubilized peptide: structural and mechanistic implications. Biophys. J. 76, 1179-1189.
- Damo, S.M., Phillips, A.H., Young, A.L., Li, S., Woods, V.L., Jr., Wemmer, D.E., 2010. Probing the conformation of a prion protein fibril with hydrogen exchange. J. Biol. Chem. 285, 32303-32311.
- del Amo, J.M., Fink, U., Reif, B., 2010. Quantification of protein backbone hydrogen-deuterium exchange rates by solid state NMR spectroscopy. J. Biomol. NMR 48, 203-212.
- Delaglio, F., Grzesiek, S., Vuister, G.W., Zhu, G., Pfeifer, J., Bax, A., 1995. NMRPipe: a multidimensional spectral processing system based on UNIX pipes. J. Biomol. NMR 6, 277-293.
- Englander, S.W., Kallenbach, N.R., 1983. Hydrogen exchange and structural dynamics of proteins and nucleic acids. Q. Rev. Biophys. 16, 521-655.

- Englander, S.W., Downer, N.W., Teitelbaum, H., 1972. Hydrogen exchange. Annu. Rev. Biochem. 41, 903-924.
- Ghetti, B., Piccardo, P., Spillantini, M.G., Ichimiya, Y., Porro, M., Perini, F., Kitamoto, T., Tateishi, J., Seiler, C., Frangione, B., Bugiani, O., Giaccone, G., Prelli, F., Goedert, M., Dlouhy, S.R., Tagliavini, F., 1996. Vascular variant of prion protein cerebral amyloidosis with τ-positive neurofibrillary tangles: The phenotype of the stop codon 145 mutation in PRNP. Proc. Natl. Acad. Sci. USA 93, 744-748.
- Goddard, T.D., Kneller, D.G., 2006. SPARKY 3, University of California, San Francisco.
- Grohe, K., Movellan, K.T., Vasa, S.K., Giller, K., Becker, S., Linser, R., 2017. Non-equilibrium hydrogen exchange for determination of H-bond strength and water accessibility in solid proteins. J. Biomol. NMR 68, 7-17.
- Helmus, J.J., Jaroniec, C.P., 2013. Nmrglue: an open source Python package for the analysis of multidimensional NMR data. J. Biomol. NMR 55, 355-367.
- Helmus, J.J., Surewicz, K., Surewicz, W.K., Jaroniec, C.P., 2010. Conformational flexibility of Y145Stop human prion protein amyloid fibrils probed by solid-state nuclear magnetic resonance spectroscopy. J. Am. Chem. Soc. 132, 2393-2403.
- Helmus, J.J., Surewicz, K., Nadaud, P.S., Surewicz, W.K., Jaroniec, C.P., 2008. Molecular conformation and dynamics of the Y145Stop variant of human prion protein in amyloid fibrils. Proc. Natl. Acad. Sci. USA 105, 6284-6289.
- Helmus, J.J., Surewicz, K., Apostol, M.I., Surewicz, W.K., Jaroniec, C.P., 2011. Intermolecular alignment in Y145Stop human prion protein amyloid fibrils probed by solid-state NMR spectroscopy. J. Am. Chem. Soc. 133, 13934-13937.
- Hoshino, M., Katou, H., Yamaguchi, K., Goto, Y., 2007. Dimethylsulfoxide-quenched hydrogen/deuterium exchange method to study amyloid fibril structure. Biochim. Biophys. Acta 1768, 1886-1899.
- Jones, E.M., Surewicz, W.K., 2005. Fibril conformation as the basis of species- and strain-dependent seeding specificity of mammalian prion amyloids. Cell 121, 63-72.
- Jones, E.M., Wu, B., Surewicz, K., Nadaud, P.S., Helmus, J.J., Chen, S., Jaroniec, C.P., Surewicz, W.K., 2011. Structural polymorphism in amyloids: New insights from studies with Y145Stop prion protein fibrils. J. Biol. Chem. 286, 42777-42784.
- Kitamoto, T., Iizuka, R., Tateishi, J., 1993. An amber mutation of prion protein in Gerstman-Straussler syndrome with mutant PrP plaques. Biochem. Biophys. Res. Commun. 192, 525-531.
- Kraus, A., Groveman, B.R., Caughey, B., 2013. Prions and the potential transmissibility of protein misfolding diseases. Annu. Rev. Microbiol. 67, 543-564.

- Kundu, B., Maiti, N.R., Jones, E.M., Surewicz, K.A., Vanik, D.L., Surewicz, W.K., 2003. Nucleation-dependent conformational conversion of the Y145Stop variant of human prion protein: Structural clues for prion propagation. Proc. Natl. Acad. Sci. USA 100, 12069-12074.
- Kuwata, K., Matumoto, T., Cheng, H., Nagayama, K., James, T.L., Roder, H., 2003. NMR-detected hydrogen exchange and molecular dynamics simulations provide structural insight into fibril formation of prion protein fragment 106-126. Proc. Natl. Acad. Sci. USA 100, 14790-14795.
- Laws, D.D., Bitter, H.L., Liu, K., Ball, H.L., Kaneko, K., Wille, H., Cohen, F.E., Prusiner, S.B., Pines, A., Wemmer, D.E., 2001. Solid-state NMR studies of the secondary structure of a mutant prion protein fragment of 55 residues that induces neurodegeneration. Proc. Natl. Acad. Sci. USA 98, 11686-11690.
- Lim, K.H., Nguyen, T.N., Damo, S.M., Mazur, T., Ball, H.L., Prusiner, S.B., Pines, A., Wemmer, D.E., 2006. Solid-state NMR structural studies of the fibril form of a mutant mouse prion peptide PrP89-143(P101L). Solid State Nucl. Magn. Reson. 29, 183-190.
- Linser, R., Fink, U., Reif, B., 2009. Probing surface accessibility of proteins using paramagnetic relaxation in solid-state NMR spectroscopy. J. Am. Chem. Soc. 131, 13703-13708.
- Luhrs, T., Ritter, C., Adrian, M., Riek-Loher, D., Bohrmann, B., Dobeli, H., Schubert, D., Riek, R., 2005. 3D structure of Alzheimer's amyloid-β(1-42) fibrils. Proc. Natl. Acad. Sci. USA 102, 17342-17347.
- Nadaud, P.S., Helmus, J.J., Kall, S.L., Jaroniec, C.P., 2009. Paramagnetic ions enable tuning of nuclear relaxation rates and provide long-range structural restraints in solid-state NMR of proteins. J. Am. Chem. Soc. 131, 8108-8120.
- Oster, C., Kosol, S., Hartlmuller, C., Lamley, J.M., Iuga, D., Oss, A., Org, M.L., Vanatalu, K., Samoson, A., Madl, T., Lewandowski, J.R., 2017. Characterization of protein-protein interfaces in large complexes by solid-state NMR solvent paramagnetic relaxation enhancements. J. Am. Chem. Soc. 139, 12165-12174.
- Peretz, D., Williamson, R.A., Legname, G., Matsunaga, Y., Vergara, J., Burton, D.R., DeArmond, S.J., Prusiner, S.B., Scott, M.R., 2002. A change in conformation of prions accompanies the emergence of a new prion strain. Neuron 34, 921-932.
- Prusiner, S.B., 1998. Prions. Proc. Natl. Acad. Sci. USA 95, 13363-13383.
- Safar, J., Wille, H., Itri, V., Groth, D., Serban, H., Torchia, M., Cohen, F.E., Prusiner, S.B., 1998. Eight prion strains have PrP<sup>Sc</sup> molecules with different conformations. Nat. Med. 4, 1157-1165.
- Sengupta, I., Nadaud, P.S., Helmus, J.J., Schwieters, C.D., Jaroniec, C.P., 2012. Protein fold determined by paramagnetic magic-angle spinning solid-state NMR spectroscopy. Nat. Chem. 4, 410-417.

- Sharpe, S., Yau, W.M., Tycko, R., 2006. Structure and dynamics of the HIV-1 Vpu transmembrane domain revealed by solid-state NMR with magic-angle spinning. Biochemistry 45, 918-933.
- Skora, L., Fonseca-Ornelas, L., Hofele, R.V., Riedel, D., Giller, K., Watzlawik, J., Schulz-Schaeffer, W.J., Urlaub, H., Becker, S., Zweckstetter, M., 2013. Burial of the polymorphic residue 129 in amyloid fibrils of prion stop mutants. J. Biol. Chem. 288, 2994-3002.
- Surewicz, W.K., Apostol, M.I., 2011. Prion protein and its conformational conversion: A structural perspective. Top. Curr. Chem. 305, 135-167.
- Surewicz, W.K., Jones, E.M., Apetri, A.C., 2006. The emerging principles of mammalian prion propagation and transmissibility barriers: Insight from studies in vitro. Acc. Chem. Res. 39, 654-662.
- Theint, T., Nadaud, P.S., Surewicz, K., Surewicz, W.K., Jaroniec, C.P., 2017a. <sup>13</sup>C and <sup>15</sup>N chemical shift assignments of mammalian Y145Stop prion protein amyloid fibrils. Biomol. NMR Assign. 11, 75-80.
- Theint, T., Nadaud, P.S., Aucoin, D., Helmus, J.J., Pondaven, S.P., Surewicz, K., Surewicz, W.K., Jaroniec, C.P., 2017b. Species-dependent structural polymorphism of Y145Stop prion protein amyloid revealed by solid-state NMR spectroscopy. Nat. Commun. 8, 753.
- Vanik, D.L., Surewicz, K.A., Surewicz, W.K., 2004. Molecular basis of barriers for interspecies transmissibility of mammalian prions. Mol. Cell 14, 139-145.
- Walsh, P., Simonetti, K., Sharpe, S., 2009. Core structure of amyloid fibrils formed by residues 106-126 of the human prion protein. Structure 17, 417-426.
- Wang, S., Shi, L., Kawamura, I., Brown, L.S., Ladizhansky, V., 2011. Site-specific solid-state NMR detection of hydrogen-deuterium exchange reveals conformational changes in a 7-helical transmembrane protein. Biophys. J. 101, L23-25.
- Wickramasinghe, N.P., Parthasarathy, S., Jones, C.R., Bhardwaj, C., Long, F., Kotecha, M., Mehboob, S., Fung, L.W.M., Past, J., Samoson, A., Ishii, Y., 2009. Nanomole-scale protein solid-state NMR by breaking intrinsic <sup>1</sup>H T<sub>1</sub> boundaries. Nat. Meth. 6 215-218.
- Yamazaki, T., Lee, W., Arrowsmith, C.H., Muhandiram, D.R., Kay, L.E., 1994. A suite of triple resonance NMR experiments for the backbone assignment of <sup>15</sup>N, <sup>13</sup>C, <sup>2</sup>H labeled proteins with high sensitivity. J. Am. Chem. Soc. 116, 11655-11666.

#### **Figure Captions**

**Figure 1.** Two dimensional  $^{15}$ N- $^{13}$ Cα correlation spectra of huPrP23-144 amyloid fibrils (blue contours) and huPrP23-144 fibrils incubated with 200 mM Cu(II)-EDTA (red contours). The spectra were recorded at 800 MHz  $^{1}$ H frequency, 11.111 kHz MAS rate and effective sample temperature of ~5  $^{\circ}$ C, with  $^{15}$ N longitudinal relaxation delays of 10 μs (A) and 2 s (B) prior to  $^{15}$ N chemical shift encoding (Nadaud et al., 2009). (C) Amide  $^{15}$ N longitudinal relaxation trajectories for representative residues in huPrP23-144 fibrils (blue circles) and the same residues in huPrP23-144 fibrils incubated with 20 mM (green circles) and 200 mM Cu(II)-EDTA (red circles). Simulated best-fit trajectories to decaying single exponentials used to determine the longitudinal  $^{15}$ N relaxation rate constants (R<sub>1</sub>) are shown as solid lines of the corresponding color. See SI Figures S1 and S2 for additional  $^{15}$ N- $^{13}$ Cα spectra and complete set of relaxation trajectories.

**Figure 2.** Two dimensional  $^{15}$ N- $^{13}$ C $\alpha$  correlation spectra of huPrP23-144 amyloid fibrils (blue contours) and huPrP23-144 fibrils subjected to H/D exchange in D<sub>2</sub>O-based phosphate buffer for 48 h (red contours). The spectra were recorded at 800 MHz  $^{1}$ H frequency, 11.111 kHz MAS rate and effective sample temperature of ~5  $^{\circ}$ C as described in the text.

**Figure 3.** (A) Plot of the longitudinal <sup>15</sup>N PRE as a function of residue number in huPrP23-144 amyloid fibrils incubated with 20 or 200 mM Cu(II)-EDTA as indicated in the legend. For each residue, the PRE was calculated by taking the difference between the <sup>15</sup>N R<sub>1</sub> for the paramagnetic and diamagnetic samples. (B) Plot of cross-peak intensity in <sup>15</sup>N-<sup>13</sup>Cα solid-state

NMR spectra as a function of residue number for huPrP23-144 fibrils following H/D exchange times of 2, 6 or 48 h in D<sub>2</sub>O based buffer as indicated in the legend, relative to the intensity of the corresponding cross-peak for a control fibril sample. (C) Plot of cross-peak intensity in <sup>15</sup>N
<sup>1</sup>H HSQC NMR spectra as a function of residue number for huPrP23-144 fibrils following H/D exchange times of 1, 6 or 24 h in D<sub>2</sub>O based buffer as indicated in the legend and dissolution in the DMSO based buffer, relative to the intensity of the corresponding cross-peak for a control fibril sample. Asterisks in plots shown in panels (A-C) indicate residues for which corresponding data could not be obtained due to the residue being a proline or otherwise not detectable in the solid-state NMR spectra. (D) Schematic structural model of the huPrP23-144 amyloid core based on the combination of solid-state NMR and fibril mass-per-length data (Theint et al., 2017b), with the approximate locations of several amino acid residues indicated for reference by red spheres.

